The model included the effects of rotation, radius change, and stream-surface convergence. An upwind-implicit approximate–factorization scheme was used to solve the turbulence model equations uncoupled from the flow equations. The numerical scheme was robust, but about 18% slower than the B–L model.

Calculations were made of a transonic compressor rotor with significant quasi-three-dimensional effects. The results showed very close agreement between the B–L and k-ω models, but both models failed to capture the measured wake spreading. Calculations were also made of a transonic turbine vane with transition and heat transfer. Both turbulence models showed very good agreement with measured surface pressures. Surface heat transfer was predicted reasonably well by the B–L model, considering the simple transition model used. The low Reynolds number k-ω model gave similar results, but the predicted transition location was sensitive to inlet values of ω. Overall the k-ω model behaved well numerically, but predictions were not decisively better than those made with the B–L model.

References

[1]Baldwin, B. S., and Lomax, H., "Thin-Layer Approximation and Algebraic Model for Separated Turbulent Flows," AIAA Paper 78-257, Jan. 1978.

[2]Wilcox, D. C., "Turbulence Modeling for CFD," DCW Industries, Inc., La Canada, CA, 1994.

[3]Wilcox, D. C., "Simulation of Transition with a Two-Equation Turbulence Model," *AIAA Journal*, Vol. 32, No. 2, 1994, pp. 247–255.

[4]Menter, F. R., "Improved Two-Equation k-ω Turbulence Model for Aerodynamic Flows," NASA TM-103975, Oct. 1992.

[5]Liu, F., and Zheng, X., "Staggered Finite Volume Scheme for Solving Cascade Flow with a k-ω Turbulence Model," *AIAA Journal*, Vol. 32, No. 8, 1994, pp. 1589–1597.

[6]Chima, R. V., "Explicit Multigrid Algorithm for Quasi-Three-Dimensional Viscous Flows in Turbomachinery," *Journal of Propulsion and Power*, Vol. 3, No. 5, 1987, pp. 397–405.

[7]Baldwin, B. S., and Barth, T. J., "A One-Equation Turbulence Transport Model for High Reynolds Number Wall-Bounded Flows," NASA TM 102847, Aug. 1990.

[8]Suder, K. L., Chima, R. V., Strazisar, A. J., and Roberts, W. B., "The Effect of Adding Thickness and Roughness to a Transonic Axial Compressor Rotor," *Journal of Turbomachinery*, Vol. 117, No. 4, 1995, pp. 491–505.

[9]Arts, T., Lambert de Rouvroit, M., and Rutherford, A. W., "Aero-Thermal Investigation of a Highly Loaded Transonic Linear Turbine Guide Vane Cascade," von Kármán Inst. for Fluid Dynamics, TN 174, Belgium, Sept. 1990.

Linear Acoustic Analysis of Solid Propellant Pressure-Coupled Distributed Combustion

Michael M. Micci*
Pennsylvania State University, University Park, Pennsylvania 16802

Nomenclature

a = speed of sound
c_p = specific heat at constant pressure
e_0 = stagnation or total internal energy
i = $\sqrt{-1}$
m_b = volumetric mass injection rate
p = pressure
R = gas constant
R_p = pressure-coupled response
R_v = velocity-coupled response
T = temperature
T_f = adiabatic flame temperature
t = time
u = gas velocity
x = distance above the propellant surface
γ = ratio of specific heats
ΔT = nonisentropic flame temperature contribution
ρ = density
ω = angular frequency

Superscripts
$'$ = perturbation quantity
$-$ = mean quantity
$\hat{}$ = complex perturbation quantity

Received Nov. 9, 1995; revision received May 6, 1996; accepted for publication June 5, 1996. Copyright © 1996 by the American Institute of Aeronautics and Astronautics, Inc. All rights reserved.

*Associate Professor, Department of Aerospace Engineering and Propulsion Engineering Research Center, 233 Hammond Building. Senior Member AIAA.

Introduction

DISTRIBUTED combustion is the term used to denote the combustion of solid particles, usually metals such as aluminum or boron, in the combustion chambers of solid propellant rocket motors after they have been emitted from the burning solid propellant surface, but before they pass through the nozzle. Beckstead[1] has shown that the unsteady particle combustion can significantly influence the rocket motor acoustic stability. Models for distributed combustion have been proposed,[2] but there currently exist no methods for experimentally measuring the unsteady distributed combustion response under conditions that simulate those found in actual solid propellant rocket motors.

However, it has been shown that in a modulated exhaust combustion chamber with solid propellant only at the head end of the chamber, in a so-called cigarette or end-burning mode, measurements of the unsteady gas velocity as functions of distance above the burning propellant surface by means of magnetic velocimetry,[3] along with measurements of the unsteady pressure, combined with a one-dimensional linear acoustic analysis of the flow within the chamber,[4] can be used to obtain the propellant pressure-coupled combustion response with a high degree of accuracy. The analysis assumed that all of the propellant combustion occurred in a region very close to the burning propellant surface, allowing the propellant response to be treated as a boundary condition. Such an assumption is valid for nonmetallized composite propellants. By modifying the acoustic analysis as described in the next section, to allow for distributed combustion away from the propellant surface, the same experimental technique can be used to measure the unsteady distributed combustion response.

Analysis

One takes the one-dimensional constant area (variable areas can be included, but are excluded here for simplicity) unsteady compressible equations for the conservation of mass, momentum, and energy with mass, momentum, and energy sources caused by the combustion of the metal particles after they are emitted from the burning solid propellant surface

$$\frac{\partial \rho}{\partial t} + \frac{\partial (\rho u)}{\partial x} = m_b \tag{1}$$

$$\frac{\partial (\rho u)}{\partial t} + \frac{\partial (\rho u^2)}{\partial x} + \frac{\partial p}{\partial x} = u m_b \tag{2}$$

$$\frac{\partial (\rho e_0)}{\partial t} + \frac{\partial (\rho u e_0)}{\partial x} + \frac{\partial (p u)}{\partial x} = c_p T_f m_b \tag{3}$$

where m_b is caused from the particle combustion.

One subtracts u times continuity from momentum to obtain

$$\rho \frac{\partial u}{\partial t} + \rho u \frac{\partial u}{\partial x} + \frac{\partial p}{\partial x} = 0 \tag{4}$$

One subtracts $u^2/2$ times continuity and u times momentum [Eq. (4)] from energy, expanding e_0 into static internal energy and kinetic energy, assuming constant specific heats and substituting the perfect gas law for density to obtain

$$\frac{\partial p}{\partial t} + u \frac{\partial p}{\partial x} + \gamma p \frac{\partial u}{\partial x} = \gamma R(T_f + \Delta T) m_b \tag{5}$$

The equations are now linearized by assuming each variable to be the sum of a mean and a small perturbation of the order of the mean Mach number of the flow, i.e., $p = \bar{p} + p'$, etc. Following Culick,[5] terms of the order M^2 and higher are dropped and T_f is written as $T + \Delta T$.

The governing equations for the mean quantities are subtracted out and solved separately. Since T' is the isentropic temperature fluctuation

$$\gamma R T' \bar{m}_b = (\gamma - 1) \frac{p'}{\bar{\rho}} \bar{m}_b = (1 - \gamma) p' \frac{\mathrm{d}\bar{u}}{\mathrm{d}x} \tag{6}$$

which is valid when terms of the order M^2 or higher are negligible, is used to eliminate T' in the energy equation.

The fluctuating components are then assumed to vary sinusoidally with time and are written as

$$p' = \hat{p}(x)e^{i\omega t}, \quad u' = \hat{u}(x)e^{i\omega t}, \quad m_b' = \hat{m}_b(x)e^{i\omega t}, \quad T' = \hat{T}(x)e^{i\omega t} \tag{7}$$

where $\hat{p}(x)$, $\hat{u}(x)$, $\hat{m}_b(x)$, and $\hat{T}(x)$ are complex numbers and contain both amplitude and phase information. Substituting into the linearized perturbation equations and dividing out $e^{i\omega t}$, one finally obtains for momentum and energy

$$i\omega\bar{\rho}\hat{u} + \bar{\rho}\hat{u} \frac{\mathrm{d}\bar{u}}{\mathrm{d}x} + \bar{\rho}\bar{u} \frac{\mathrm{d}\hat{u}}{\mathrm{d}x} + \frac{\mathrm{d}\hat{p}}{\mathrm{d}x} = 0 \tag{8}$$

$$i\omega\hat{p} + \bar{u} \frac{\mathrm{d}\hat{p}}{\mathrm{d}x} + \hat{u} \frac{\mathrm{d}\bar{p}}{\mathrm{d}x} + \gamma\bar{p} \frac{\mathrm{d}\hat{u}}{\mathrm{d}x} + \hat{p} \frac{\mathrm{d}\bar{u}}{\mathrm{d}x} = \bar{a}^2 \bar{m}_b \left[\frac{\hat{m}_b}{\bar{m}_b} + \frac{\Delta\hat{T}}{\bar{T}} \right]$$
$$= \bar{a}^2 \bar{m}_b \left(R_p \frac{\hat{p}}{\bar{p}} + R_v \frac{\hat{u}}{\bar{a}} \right) \tag{9}$$

where

$$R_p = \left[\frac{\hat{m}_b}{\bar{m}_b} + \frac{\Delta\hat{T}}{\bar{T}} \right] \Big/ \frac{\hat{p}}{\bar{p}} \tag{10a}$$

$$R_v = \left[\frac{\hat{m}_b}{\bar{m}_b} + \frac{\Delta\hat{T}}{\bar{T}} \right] \Big/ \frac{\hat{u}}{\bar{a}} \tag{10b}$$

The term within the brackets in Eq. (9) is the sum of the nondimensionalized unsteady mass and energy injection caused by unsteady particle combustion, and R_p and R_v are the pressure- and velocity-coupled responses, respectively, of the particle combustion. Equations (8) and (9) are then simultaneously solved numerically along with the steady-state equations for mass, momentum, and energy as initial value problems in a manner similar to Ref. 6, starting at the head end of the chamber where a pressure oscillation of arbitrary, but small, magnitude (relative to the mean pressure) and a velocity oscillation given by the propellant pressure-coupled response are applied. The governing equations are solved in this manner to allow arbitrary spatial distributions for both the steady and unsteady particle combustion. The initial values for the steady-state equations are the head-end mean pressure, the mean velocity of the gas produced by the solid propellant combustion, and the mean density at the head end obtained from the adiabatic flame temperature and the perfect gas law. Since the flow within the chamber is one dimensional, only longitudinal mode acoustic waves are modeled. Since the flow region above an end-burning grain is being solved for, the pressure- and velocity-coupled responses in the last term in Eq. (9) are for the distributed combustion alone. *Mathematica* was used to compute and plot the results.

Results

Figure 1 shows the velocity oscillation phase angle relative to the head-end pressure oscillation as a function of distance above the burning surface for three values of the real part of the solid propellant pressure-coupled response (1, 3, and 5) without distributed combustion. The modulation frequency is 1000 Hz. When the pressure-coupled response is one, the admittance at the surface is zero and the phase angle is 90 deg, produced by a classical acoustic wave modified by the low Mach number mean flow within the chamber. The other solutions show that for nonunity real parts (only the real part affects the growth or decay of acoustic waves within the chamber), the velocity phase angle shows dramatically altered behavior in the region near the burning propellant surface and that the magnitude of this effect is roughly proportional to the magnitude of the real part. It is this velocity phase angle behavior that is measured in a magnetic flowmeter burner to obtain the real part of the pressure-coupled response. The imaginary part was found to have no effect on the phase angle.

Figure 2 shows the effect of a nonzero real part of the distributed combustion response on the velocity oscillation phase angle for the same modulation frequency of 1000 Hz. For all three cases shown, the real part of the propellant pressure-coupled response has a value of 2. It can be seen in case B where the real part of the distributed combustion pressure-coupled response equals 10 that distributed combustion shifts the velocity phase angle away from 90 deg by an amount proportional to the magnitude of the real part. Case C shows that this shift begins where the distributed combustion begins to occur and that by measuring the velocity oscillation phase angle as a function of distance above the burning propellant surface one can deduce the magnitude of the real part of the distributed combustion response and where it occurs relative to the burning propellant surface. The imaginary part of the pressure-coupled response was found to have a very weak effect on the velocity phase angle. Both the real and imaginary parts of the velocity-coupled distributed combustion response were found to have no effect on the velocity phase angle since the acoustic oscillations are being modeled in the vicinity of

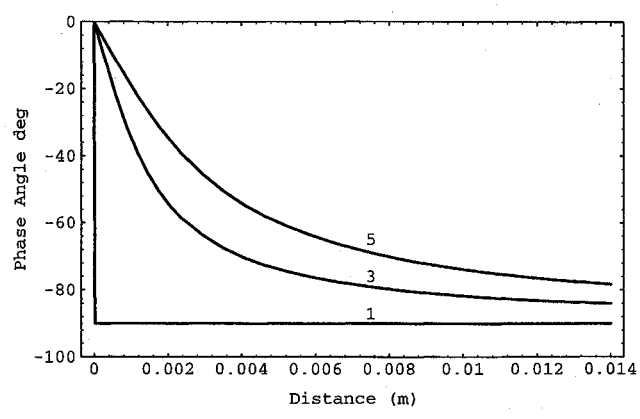

Fig. 1 Phase angle of the velocity oscillation as a function of distance above the solid propellant surface without distributed combustion for three values of the real part of the solid propellant pressure-coupled response.

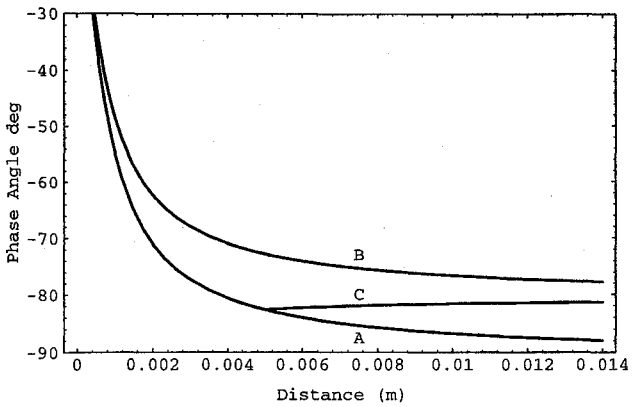

Fig. 2 Phase angle of the velocity oscillation as a function of distance above the propellant surface for three values of the real part of the distributed combustion response: A, 0.0; B, 10.0 starting at the propellant surface; and C, 10.0 starting at 5 mm above the surface.

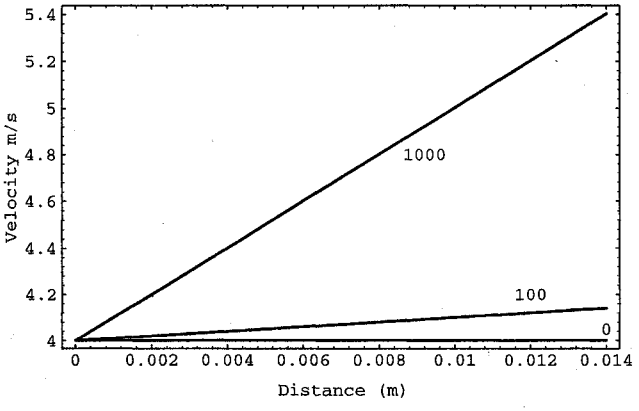

Fig. 3 Gas velocity as a function of distance above the propellant surface for three values of the volumetric mass release rate caused from distributed combustion.

a velocity node. Therefore, one can obtain the pressure-coupled distributed combustion response without any experimental ambiguity being introduced by the velocity-coupled response; the disadvantage is that no information on the velocity-coupled distributed combustion response would be obtained. Since the spatial resolution of a magnetic flowmeter is given by the electrode diameter (0.5 mm), the analysis shows that a magnetic flowmeter burner can measure the magnitude and location of the real part of the pressure-coupled distributed combustion response.

The steady-state equations can also be used to study the effect of the steady-state distributed combustion on the flow within the burner. Figure 3 shows the effect of three values for the steady-state volumetric mass release rate resulting from distributed combustion (0, 100, and 1000 kg/m^3 s) on the mean gas velocity above the propellant surface. The volumetric mass release caused from distributed combustion causes an increase in the mean gas velocity, which is large enough to be measured by a magnetic flowmeter, thus allowing the determination of the location and magnitude of the steady-state distributed combustion. If one assumes that the products of distributed combustion consist of condensed phases only with the result that heat addition is the only source in the governing equations, similar effects for both the steady and unsteady flowfields are found.

References

[1]Beckstead, M. W., "Evidences for Distributed Combustion," *24th JANNAF Combustion Meeting*, Vol. 1 (Monterey, CA), Chemical Propulsion Information Agency, Columbia, MD, 1987, pp. 1–12.

[2]Brooks, K. P., and Beckstead, M. W., "Dynamics of Aluminum Combustion," *Journal of Propulsion and Power*, Vol. 11, No. 4, 1995, pp. 769–780.

[3]Wilson, J. R., and Micci, M. M., "Direct Measurement of High Frequency, Solid Propellant, Pressure-Coupled Admittances," *Journal of Propulsion and Power*, Vol. 3, No. 4, 1987, pp. 296–302.

[4]Cauty, F., Comas, P., Vuillot, F., and Micci, M. M., "Magnetic Flow Meter Measurement of Solid Propellant Pressure-Coupled Responses Using an Acoustic Analysis," *Journal of Propulsion and Power*, Vol. 12, No. 2, 1996, pp. 436–438.

[5]Culick, F. E. C., "The Stability of One-Dimensional Motions in a Rocket Motor," *Combustion Science and Technology*, Vol. 7, No. 4, 1973, pp. 165–175.

[6]Micci, M. M., Caveny, L. H., and Sirignano, W. A., "Linear Analysis of Forced Longitudinal Waves in Rocket Motor Chambers," *AIAA Journal*, Vol. 19, No. 2, 1981, pp. 198–204.

Impulse Function and Drag in Scramjet Inlet Models

Takeshi Kanda,* Kouichiro Tani,*
Tomoyuki Komuro,† Atsuo Murakami,†
Kenji Kudo,† and Nobuo Chinzei‡
National Aerospace Laboratory, Miyagi 981-15, Japan

Introduction

In a typical airframe-integrated scramjet, for example, the NASA Langley-type scramjet, the side walls in the inlet function as a compression system. The inlet has a bottomless geometry, and sometimes has a swept angle to guarantee startability. The open bottom results in spillage and the swept angle increases it. To discuss engine performances, appropriate estimation of drags in such an inlet, including the spillage of mass and momentum, is required.

The shock-wave relation can be applied to analyze the airflow in the inlet. However, estimation based on this relation does not include the end effect of the wall or the open bottom. Furthermore, when the inflow Mach number is low, or the swept angle is large, the velocity component, which the shock-wave relation is applied to, becomes subsonic.[1] To date, there have been relatively few experiments and numerical simulations investigating the characteristics of the inlet drag and those of the spilled air, and consequently, there are few reports dealing with these characteristics.[2–4]

In the present study, several kinds of side-wall compression-type inlets were tested, and the impulse function and the drag in the inlet models with spillage were investigated.

Experimental Apparatus

A blow-down-type Mach 4.1 wind tunnel was used in the present testing.[1] The total pressure and the total temperature of the working fluid, air, were 1.6 MPa, and 290 K, respec-

Received Oct. 5, 1995; revision received June 4, 1996; accepted for publication June 4, 1996. Copyright © 1996 by the American Institute of Aeronautics and Astronautics, Inc. All rights reserved.

*Senior Researcher, Kakuda Research Center, Ramjet Propulsion Research Division, Kimigaya, Kakuda. Member AIAA.

†Senior Researcher, Kakuda Research Center, Ramjet Propulsion Research Division, Kimigaya, Kakuda.

‡Head, Ramjet Performance Section, Kakuda Research Center, Ramjet Propulsion Research Division, Kimigaya, Kakuda. Member AIAA.